

## THE RELATIONSHIP BETWEEN MOLECULAR GAS TRACERS AND KENNICUTT-SCHMIDT LAWS

MARK R. KRUMHOLZ<sup>1</sup> AND TODD A. THOMPSON<sup>2</sup>

Department of Astrophysical Sciences, Princeton University, Princeton, NJ 08544;  
 krumholz@astro.princeton.edu, thomp@astro.princeton.edu

Received 2007 March 30; accepted 2007 July 16

### ABSTRACT

We provide a model for how Kennicutt-Schmidt (KS) laws, which describe the correlation between star formation rate and gas surface or volume density, depend on the molecular line chosen to trace the gas. We show that, for lines that can be excited at low temperatures, the KS law depends on how the line critical density compares to the median density in a galaxy’s star-forming molecular clouds. High critical density lines trace regions with similar physical properties across galaxy types, and this produces a linear correlation between line luminosity and star formation rate. Low critical density lines probe regions whose properties vary across galaxies, leading to a star formation rate that varies super-linearly with line luminosity. We show that a simple model in which molecular clouds are treated as isothermal and homogenous can quantitatively reproduce the observed correlations between galactic luminosities in far-infrared and in the CO(1→0) and HCN(1→0) lines, and naturally explains why these correlations have different slopes. We predict that IR-line luminosity correlations should change slope for galaxies in which the median density is close to the line critical density. This prediction may be tested by observations of lines such as HCO<sup>+</sup>(1→0) with intermediate critical densities, or by HCN(1→0) observations of intensely star-forming high-redshift galaxies with very high densities. Recent observations by Gao et al. hint at just such a change in slope. We argue that deviations from linearity in the HCN(1→0)–IR correlation at high luminosity are consistent with the assumption of a constant star formation efficiency.

*Subject headings:* galaxies: ISM — ISM: clouds — ISM: molecules — radio lines: ISM — stars: formation

### 1. INTRODUCTION

Schmidt (1959, 1963) first proposed that the rate at which a gas forms stars might follow a simple power-law correlation of the form  $\dot{\rho}_* \propto \rho_g^N$ , where  $\dot{\rho}_*$  is the star formation rate per unit volume,  $\rho_g$  is the gas density, and  $N$  is generally taken to be in the range 1–2. In the decades since, observations have revealed two strong correlations that appear to be evidence for this hypothesis. First, galaxy surveys reveal that the infrared luminosity of a galaxy, which traces the star formation rate, varies with its luminosity in the CO(1→0) line, which traces the total mass of molecular gas, as  $L_{\text{FIR}} \propto L_{\text{CO}}^{1.4-1.6}$  (Gao & Solomon 2004a, 2004b; Greve et al. 2005; Riechers et al. 2006a). Kennicutt (1998a, 1998b) identified the closely related correlation between gas surface density  $\Sigma_g$  and star formation rate surface density  $\Sigma_*$ ,  $\Sigma_* \propto \Sigma_g^{1.4 \pm 0.15}$ , a relation that has come to be known as the Kennicutt law. Since over the bulk of the dynamic range of Kennicutt’s data, galaxies are predominantly molecular, this is effectively a correlation between molecular gas, as traced by CO(1→0) line emission, and star formation. Spatially resolved observations of galaxies confirm that, at least for molecule-rich galaxies where resolved CO(1→0) observations are possible, star formation is more closely coupled with gas traced by CO(1→0) than with atomic gas (Wong & Blitz 2002; Heyer et al. 2004; Komugi et al. 2005; Kennicutt et al. 2007).

Second, Gao & Solomon (2004a, 2004b) found that there is a strong correlation between the IR luminosity of galaxies and emission in the HCN(1→0) line, which measures the mass at densities significantly greater than that probed by CO(1→0). However, they find that their correlation, which covers nearly three decades in total galactic star formation rate, is linear:  $L_{\text{FIR}} \propto L_{\text{HCN}}$ . Wu et al. (2005) showed that this correlation extends down to individual star-forming clumps of gas in the Milky Way, provided that their in-

frared luminosities are  $\gtrsim 10^{4.5} L_\odot$ . Interestingly, however, Gao et al. (2007) found a deviation from linearity in the IR-HCN correlation for a sample of intensely star-forming high-redshift galaxies. These sources show small but significant excesses of infrared emission for their observed HCN emission.

The difference in power-law indices between the  $L_{\text{FIR}}-L_{\text{CO}}$  and  $L_{\text{FIR}}-L_{\text{HCN}}$  correlations is statistically significant and, on its face, puzzling. An index near  $N = 1.5$  seems natural if one supposes that a roughly constant fraction of the gas present in molecular clouds will be converted into stars each free-fall time. In this case, one expects  $\dot{\rho}_* \propto \rho_g^{1.5}$  (Madore 1977; Elmegreen 1994). If gas scale heights do not vary strongly from galaxy to galaxy, this implies  $\Sigma_* \propto \Sigma_g^{1.5}$  as well, which is consistent with the observed Kennicutt law. More generally, since the dynamical timescale in a marginally Toomre-stable ( $Q \approx 1$ ; see Martin & Kennicutt 2001) galactic disk is of order  $\Omega^{-1} \propto (G\rho_g)^{-1/2}$ , where  $\Omega$  is the angular frequency of the disk, an index close to  $N = 1.5$  is expected if star formation is regulated by any phenomenon that converts a fixed fraction of the gas into stars on this timescale (Elmegreen 2002).

On the other hand, Wu et al. (2005) suggested a simple interpretation of the linear IR-HCN correlation. They argue that the individual HCN-emitting molecular clumps that they identify in the Milky Way represent a fundamental unit of star formation. The linear correlation between star formation rate and HCN luminosity across galaxies arises because a measurement of the HCN luminosity for a galaxy simply counts the number of such structures present within it, each of which forms stars at some roughly fixed rate regardless of its galactic environment. However, in this interpretation it is unclear why the structures traced by HCN(1→0) emission should form stars at the same rate in any galaxy. After all, one could equally well argue that molecular clouds traced by CO(1→0) are fundamental units of star formation, but the non-linear IR-CO correlation clearly shows that these objects do not form stars at a fixed rate per unit mass. Moreover, the evidence presented by Gao et al. (2007) that the linear IR-HCN correlation

<sup>1</sup> Hubble Fellow.

<sup>2</sup> Lyman Spitzer Jr. Fellow.

varies in extremely luminous high-redshift galaxies suggests that the relationship between HCN emission and star formation may be somewhat more complex.

In this paper we attempt to explain the origin of the difference in slope between the CO and HCN correlations with star formation rate, and more generally to give a theoretical framework for understanding how correlations between star formation rate and line luminosity, which we generically refer to as KS laws, depend on the tracer used to define them. Our central argument is conceptually quite simple, and in some sense represents a combination of the intuitive arguments for CO and HCN given above.

Consider an observation of a galaxy in a molecular tracer with critical density  $n_{\text{crit}}$ , which essentially measures the mass of gas at densities of  $n_{\text{crit}}$  or more, i.e., the gas that is dense enough for that particular transition to be excited. In galaxies where the median density of the molecular gas is significantly larger than  $n_{\text{crit}}$ , this means that the observation will detect the majority of the gas, and the bulk of the emission will come from gas whose density is near the median density. Since the gas density will vary from galaxy to galaxy, the star formation rate per unit gas mass will vary as roughly  $\rho_g^{1.5}$ , with one factor of  $\rho_g$  coming from the amount of gas available for star formation, and an additional factor of  $\rho_g^{0.5}$  coming from the dependence of the free fall or dynamical time on the density.

On the other hand, in galaxies where the median gas density is small compared to the critical density for the chosen transition, observations will pick out only high-density peaks. Since the density in these peaks is set by  $n_{\text{crit}}$  and not by the conditions in the galaxy, these peaks are at essentially the same density in any galaxy where they are observed, and the corresponding free-fall times in these regions are constant as well. As a result, the star formation rate per unit mass of gas traced by that line is approximately the same in every galaxy, because the corresponding free-fall time is the same in every galaxy.

In the rest of this paper, we give a quantitative version of this intuitive argument and then discuss its consequences. In § 2 we develop a simple formalism to compute the star formation rate and the molecular line luminosity of galaxies, and in § 3 we use this formalism to predict the correlation between star formation rate and luminosity. We show that our predictions provide a very good fit for a variety of observations, and make predictions for future observations. We discuss the implications of our work and its limitations in § 4, and summarize our conclusions in § 5.

## 2. STAR FORMATION RATES AND LINE LUMINOSITIES

### 2.1. Cloud Properties

Consider a galaxy in which the star-forming molecular clouds have a volume-averaged mean molecular hydrogen number density  $\bar{n} = \bar{\rho}_g / \mu_{\text{H}_2}$ , where  $\bar{\rho}_g$  is the volume-averaged mass density of the molecular clouds in the galaxy and  $\mu_{\text{H}_2} = 3.9 \times 10^{-24}$  g is the mean mass per hydrogen molecule for a gas of standard cosmic composition. Observations indicate that  $\bar{n}$  varies by two to three decades over the galaxies for which the Kennicutt and Gao & Solomon correlations are measured, from  $\bar{n} \approx 50 \text{ cm}^{-3}$  in normal spirals like the Milky Way (McKee 1999) up to  $\bar{n} \approx 10^4 \text{ cm}^{-3}$  in the strongest starburst systems in the local universe (e.g., Downes & Solomon 1998). There is strong evidence that densities in molecular clouds follow a lognormal probability distribution function (PDF; see reviews by Mac Low & Klessen [2004] and Elmegreen & Scalo [2004]),

$$\frac{dp}{d \ln x} = \frac{1}{\sqrt{2\pi\sigma^2}} \exp\left[-\frac{(\ln x - \overline{\ln x})^2}{2\sigma^2}\right], \quad (1)$$

where  $x = n/\bar{n}$  is the molecular hydrogen number density  $n$  relative to the average density,  $\sigma$  is the width of the lognormal, and  $\overline{\ln x} = -\sigma^2/2$ . For this distribution the median density is  $n_{\text{med}} = \bar{n} \exp(\sigma^2/2)$ . Numerical experiments show that for supersonic isothermal turbulence  $\sigma^2 \approx \ln(1 + 3\mathcal{M}^2/4)$ , where  $\mathcal{M}$  is the one-dimensional Mach number of the turbulence (Nordlund & Padoan 1999; Ostriker et al. 1999; Padoan & Nordlund 2002). Mach numbers in star-forming molecular clouds range from  $\mathcal{M} \sim 30$  (McKee 1999) in normal spirals to  $\mathcal{M} \sim 100$  in strong starbursts (Downes & Solomon 1998), implying that median densities in molecular clouds range from  $\sim 10^3 \text{ cm}^{-3}$  in normal spirals to  $\sim 10^6 \text{ cm}^{-3}$  in starbursts. Star-forming clouds within a galaxy are approximately isothermal, except very near strong sources of stellar radiation, so we assume a fixed temperature  $T$  for the clouds. Observationally,  $T$  ranges from roughly 10 K in normal spirals (McKee 1999) up to as much as about 50 K in strong starbursts (Downes & Solomon 1998; Gao & Solomon 2004b).

### 2.2. Star Formation Rates

First let us ask how quickly stars form in such a medium. Krumholz & McKee (2005) gave a model for star formation regulated by supersonic turbulence in which a population of molecular clouds of total mass  $M_{\text{cl}}$  form stars at a rate  $\dot{M}_* = \text{SFR}_{\text{ff}} M_{\text{cl}} / t_{\text{ff}}(\bar{n})$ , where  $t_{\text{ff}}(\bar{n})$  is the free-fall time evaluated at the mean density and  $\text{SFR}_{\text{ff}}$  is a number of order  $10^{-2}$  that depends weakly on  $\mathcal{M}$ . We therefore estimate the star formation rate per unit volume as a function of the mean density given by

$$\dot{\rho}_* \approx \text{SFR}_{\text{ff}} \sqrt{\frac{32G\mu_{\text{H}_2}^3 \bar{n}^3}{3\pi}}. \quad (2)$$

We adopt the Krumholz & McKee result  $\text{SFR}_{\text{ff}} \approx 0.014(\mathcal{M}/100)^{-0.32}$  for clouds with a fiducial virial ratio of  $\alpha_{\text{vir}} = 1.3$ .

Alternately, Krumholz & Tan (2007) pointed out that observed correlations between the star formation rate and the luminosity in different density tracers imply that over a 3–4 decade range in density  $n$ ,

$$\dot{M}_* \approx 10^{-2} \frac{M_{\text{cl}}(>n)}{t_{\text{ff}}(n)}, \quad (3)$$

where  $M_{\text{cl}}(>n)$  is the mass of gas with a density of  $n$  or higher, and  $M_{\text{cl}} = M_{\text{cl}}(>0)$ . For a given choice of  $n$  this provides an alternative estimate of the star formation rate that is purely empirical and independent of any particular theoretical model. However, the difference between the star formation rates predicted by equations (2) and (3) is small. For gas with a lognormal PDF,

$$M_{\text{cl}}(>n) = \frac{M_{\text{cl}}}{2} \left[ 1 + \text{erf}\left(\frac{-2 \ln x + \sigma^2}{2^{3/2}\sigma}\right) \right], \quad (4)$$

and using this to evaluate equation (3) indicates that for Mach numbers in the observed range, the two prescriptions (2) and (3) give about the same star formation rate over a very broad range in  $x$ . For example, at  $\mathcal{M} = 30$  the two estimates agree to within a factor of 3 for densities in the range  $0.2 < x < 4 \times 10^4$ . Given the scatter inherent in observational estimates of the star formation rate, a factor of 3 difference is not particularly significant, so it matters little which prescription we adopt. In practice, we will use equation (2).

### 2.3. Line Luminosities

Now we must compute the luminosity of molecular line emission from the galaxy. Even for a cloud that is not in local thermodynamic

equilibrium (LTE), for optically thin emission this calculation is straightforward. However, the molecular lines used most often in galaxy surveys are generally optically thick. To handle the effect of finite optical depth on molecule level populations and line luminosities, we adopt an escape probability approximation and treat clouds as homogeneous spheres. This is not fully consistent with our assumption that clouds have lognormal density PDFs, since the escape probability formalism assumes a uniform level population throughout the cloud, and the essence of our argument in this paper turns on how the level population varies with density. However, this approach gives us an approximate way of incorporating the optical thickness of star-forming clouds into our model, the only alternative to which, for turbulent media, is full numerical simulation (e.g., Juvela et al. 2001). We therefore proceed by treating clouds as homogeneous in order to determine their escape probabilities, and we then relax the assumption of homogeneity while keeping the escape probabilities fixed, in order to determine level populations and cloud luminosities as a function of density.

Consider a cloud of radius  $R$  in statistical equilibrium but not necessarily in LTE. In the escape probability approximation, the fraction  $f_i$  of molecules of species  $S$  in state  $i$  is given implicitly by the linear system

$$\sum_j (nq_{ji} + \beta_{ji}A_{ji})f_j = \left[ \sum_j (nq_{ij} + \beta_{ij}A_{ij}) \right] f_i, \quad (5)$$

$$\sum_i f_i = 1, \quad (6)$$

where  $q_{ij}$  is the collision rate for transitions from state  $i$  to state  $j$ ,  $A_{ij}$  is the Einstein spontaneous emission coefficient for this transition,  $\beta_{ij}$  is the cloud-averaged escape probability for photons emitted in this transition, the sums are over all quantum states, and we understand that  $A_{ij} = 0$  for  $i \leq j$  and that  $q_{ij} = 0$  for  $i = j$ .

Equations (5) and (6) allow us to compute the level populations  $f_i$  for given values of  $\beta_{ij}$ . To completely specify the system, we must add an additional consistency condition relating the values of  $\beta_{ij}$  to the level populations. For a homogeneous spherical cloud, the escape probability for a given line is related to the optical depth from the center to the edge of the cloud  $\tau_{ij}$  by (B. Draine 2007, private communication)

$$\beta_{ij} \approx \frac{1}{1 + 0.5\tau_{ij}}, \quad (7)$$

where  $\tau_{ij}$  is computed at the central frequency of the line. In turn, the optical depth is related to the level populations by

$$\tau_{ij} = \frac{g_i}{g_j} \frac{A_{ij}\lambda_{ij}^3}{4(2\pi)^{3/2}\mathcal{M}c_s} \bar{n}X(S)f_jR \left( 1 - \frac{f_i g_j}{f_j g_i} \right), \quad (8)$$

where  $\lambda_{ij}$  is the wavelength of transition  $i \rightarrow j$ ,  $g_i$  and  $g_j$  are the statistical weights of states  $i$  and  $j$ ,  $c_s$  is the isothermal sound speed of the gas, and  $X(S)$  is the abundance of molecules of species  $S$ . Note that this equation implicitly assumes that the cloud has a uniform Maxwellian velocity distribution with one-dimensional dispersion  $\mathcal{M}c_s$ , consistent with our treatment of the clouds as homogeneous spheres. One additional complication is that we do not directly know cloud radii for most external galaxies, where observations cannot resolve individual molecular clouds. However, we often can diagnose the optical depths of transitions by comparing line ratios of molecular isotopomers of

different abundances. We therefore take  $\tau_{10}$ , the optical depth of the transition between the first excited state and the ground state, as known. For a given level population this fixes the value of  $R$ .

We solve equations (5)–(8) using Newton-Raphson iteration. In this procedure, we guess an initial set of escape probabilities  $\beta_{ij}$ , and solve the linear system (5) and (6) to find the corresponding initial level populations  $f_i$ . We then compute the optical depths  $\tau_{ij}$  from equation (8). The guessed escape probabilities  $\beta_{ij}$  and the corresponding optical depths  $\tau_{ij}$  generally will not satisfy the consistency condition (7), so we then iterate over  $\beta_{ij}$  values using a Newton-Raphson approach, seeking  $\beta_{ij}$  for which the level populations give optical depths  $\tau_{ij}$  such that all elements of the matrix  $\beta_{ij} - 1/(1 + 0.5\tau_{ij})$  are equal to zero within some specified tolerance. We use the LTE level populations and escape probabilities for our initial guess so that the iteration converges rapidly when the system is close to LTE.

Once we have determined the escape probabilities  $\beta_{ij}$ , we compute the luminosity by holding the  $\beta_{ij}$  values fixed but allowing the level populations to vary with density, then integrating over the PDF. Thus, the total luminosity per unit volume in a particular line is

$$L_{ij} = X(S)\beta_{ij}A_{ij}h\nu_{ij} \int_{-\infty}^{\infty} f_i n \frac{dp}{d \ln x} d \ln x, \quad (9)$$

where  $\nu_{ij}$  is the line frequency,  $f_i$  is an implicit function of  $n$  given by the solution to equations (5) and (6), and we assume that the abundance  $X(S)$  is independent of  $n$ . The line luminosity per unit mass is  $L_{ij}/(\mu_{\text{H}_2}\bar{n})$ .<sup>3</sup>

### 3. CORRELATIONS AND KS LAWS

#### 3.1. Lines and Parameters

Using the formalism of § 2, we can now predict the correlation between the star formation rate and the luminosity of a galaxy in molecular lines. We make these predictions for three representative molecular lines: CO(1→0), HCO<sup>+</sup>(1→0), and HCN(1→0). For the first and last of these transitions, there are extensive observational surveys. We select HCO<sup>+</sup>(1→0) in addition to these two because there is some observational data for it, and because its critical density of  $n_{\text{crit}} = \beta_{\text{HCO}^+}(4.6 \times 10^4) \text{ cm}^{-3}$  makes it intermediate between CO(1→0), with  $n_{\text{crit}} = \beta_{\text{CO}}560 \text{ cm}^{-3}$ , and HCN(1→0), with  $n_{\text{crit}} = \beta_{\text{HCN}}(2.8 \times 10^5) \text{ cm}^{-3}$ .<sup>4</sup> Here  $\beta_S$  is the escape probability for the 1→0 transition of species  $S$ . These critical densities are for  $T = 20$  K. All molecular data are taken from the Leiden Atomic and Molecular Database (Schöier et al. 2005).<sup>5</sup>

We make our calculations for three sets of fiducial parameters, which we summarize in Table 1. The three sets correspond roughly to typical conditions in normal disk galaxies like the Milky Way, to starburst galaxies like Arp 220, and to a case intermediate between the two. We have selected parameters for each case to roughly model the systematic variation of ISM parameters as one moves from normal disk galaxies to starbursts. Thus, we vary the ISM temperature from 10 to 50 K and the molecular cloud Mach

<sup>3</sup> An IDL code that implements this calculation is available for public download from <http://www.astro.princeton.edu/~krumholz/astrometry.html>.

<sup>4</sup> Note that our critical density for HCN(1→0) is somewhat larger than the value quoted by Gao & Solomon (2004a, 2004b) probably because their calculation is based on somewhat different assumptions about how to extrapolate from calculated rate coefficients for HCN collisions with He to collisions with H<sub>2</sub>. See Schöier et al. (2005) for details.

<sup>5</sup> See <http://www.strw.leidenuniv.nl/~moldata>.

TABLE 1  
MODEL PARAMETERS

Parameter	Normal Galaxy	Intermediate	Starburst	Reference
$T$ .....	10	20	50	1–4
$\mathcal{M}$ .....	30	50	80	1–4
$X(\text{CO})$ .....	$2 \times 10^{-4}$	$4 \times 10^{-4}$	$8 \times 10^{-4}$	5
$X(\text{HCO}^+)$ .....	$2 \times 10^{-9}$	$4 \times 10^{-9}$	$8 \times 10^{-9}$	6, 7
$X(\text{HCN})$ .....	$1 \times 10^{-8}$	$2 \times 10^{-8}$	$4 \times 10^{-8}$	6, 7, 8
$\tau_{\text{CO}(1 \rightarrow 0)}$ .....	10	20	40	9
$\tau_{\text{HCO}^+(1 \rightarrow 0)}$ .....	0.5	1.0	2.0	6, 7
$\tau_{\text{HCN}(1 \rightarrow 0)}$ .....	0.5	1.0	2.0	6, 7
OPR.....	0.25	0.25	0.25	10

NOTE.—OPR = H<sub>2</sub> ortho- to para-ratio.

REFERENCES.—(1) Solomon et al. 1987; (2) Gao & Solomon 2004b; (3) Downes & Solomon 1998; (4) Wu et al. 2005; (5) Black 2000; (6) Nguyen et al. 1992; (7) Wild et al. 1992; (8) Lahuis & van Dishoeck 2000; (9) Combes 1991; (10) Neufeld et al. 2006.

number from 30 to 80 as we move from Milky Way–like molecular clouds to temperatures and Mach numbers typical of starbursts (e.g., Downes & Solomon 1998). Similarly, starbursts, which preferentially occur at galactic centers, have systematically larger metallicities than galaxies like the Milky Way (e.g., Zaritsky et al. 1994; Yao et al. 2003; Netzer et al. 2005). To explore this effect, we use abundances and 1→0 optical depths that are 2 and 4 times as large for our intermediate and starburst models, respectively, as for our normal galaxy model.

### 3.2. KS Laws

We first plot, in Figure 1, the quantities  $L^{-1}[dL(<n)/d \ln n]$  (solid lines) and  $M^{-1}[dM(<n)/d \ln n]$  (dotted lines) as a function of density  $n$  for galaxies with mean densities  $\bar{n} = 10^2$ ,  $10^3$ , and  $10^4 \text{ cm}^{-3}$ , for the tracers CO(1→0), HCO<sup>+</sup>(1→0), and HCN(1→0), and for the Mach number and temperature corresponding to our intermediate case in Table 1. Here  $L(<n)$  and  $M(<n)$  are the luminosity and mass per unit volume contributed by gas of density  $n$  or less; i.e.,  $L(<n) = X(S)\beta_{ij}A_{ij}h\nu_{ij} \int_{-\infty}^{\ln n} f_i n \times (dp/d \ln n) d \ln n$ ,  $M(<n) = \int_{-\infty}^{\ln n} \mu_{\text{H}_2} n (dp/d \ln n) d \ln n$ ,  $L = L(<\infty)$ , and  $M = M(<\infty)$ . Physically,  $L^{-1}[dL(<n)/d \ln n]$  and  $M^{-1}[dM(<n)/d \ln n]$  represent the fractional contribution to the total line luminosity and the total mass that comes from each unit interval in the logarithm of density. The plot shows what density range provides the dominant contribution to the line luminosity in different lines and for galaxies of differing mean densities, and how the gas contributing light compares to the gas contributing mass. Because the mass distribution is entirely specified by  $\bar{n}$  and  $\mathcal{M}$ , the dotted lines are the same in each of the three panels. In addition, because of our choice  $\mathcal{M} = 50$  (Table 1), the median density {the density corresponding to the peak in  $M^{-1}[dM(<n)/d \ln n]$ } is  $n_{\text{med}} \approx 43\bar{n}$ . In each panel, the critical density for each molecule is identified by a vertical dashed line.

Figure 1 (top) clearly shows that for the CO line, the light and the mass track each other very closely, even at the lowest densities. Thus, because  $n_{\text{med}} > n_{\text{crit}}$ , the solid lines move in lock-step with the dashed lines as  $\bar{n}$  increases. In contrast, for HCN, most of the luminosity comes from densities near the critical density regardless of the mass distribution. For the lowest  $\bar{n}$  this means that the line luminosity is entirely dominated by the high-density tail of the mass distribution. As the median density  $n_{\text{med}}$  varies by a factor of 100 (from  $4.3 \times 10^3$  to  $4.3 \times 10^5 \text{ cm}^{-3}$ ), the peak of  $L^{-1}[dL(<n)/d \ln n]$  moves by just a factor of a few in  $n$ . The HCO<sup>+</sup> line is intermediate between CO and HCN. For  $\bar{n} = 10^2$  and  $10^3 \text{ cm}^{-3}$ ,  $n_{\text{med}} \lesssim n_{\text{crit}}$ , and as with HCN most of the emission

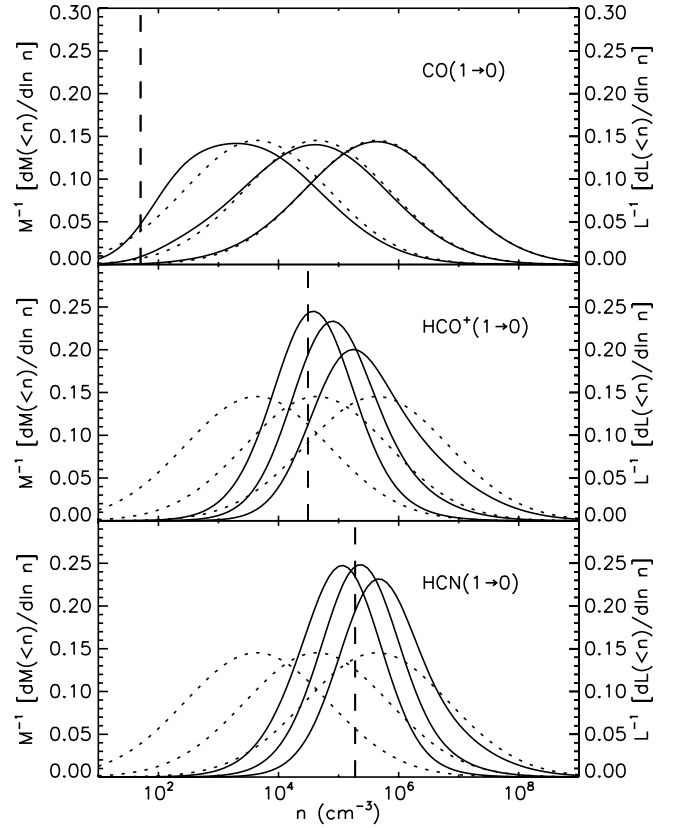


FIG. 1.—Fractional contribution to the total luminosity  $L^{-1}[dL(<n)/d \ln n]$  (solid lines) and mass  $M^{-1}[dM(<n)/d \ln n]$  (dotted lines) vs. density  $n$  for the lines CO(1→0) (top), HCO<sup>+</sup>(1→0) (middle), and HCN(1→0) (bottom). The three curves show the cases  $\bar{n} = 10^2$ ,  $10^3$ , and  $10^4 \text{ cm}^{-3}$ , from leftmost to rightmost. We also show the critical density of each molecule, corrected for radiative trapping (dashed vertical lines). These calculations use the parameters for the intermediate case listed in Table 1.

comes from near the critical density. For  $\bar{n} = 10^4 \text{ cm}^{-3}$ ,  $n_{\text{med}} > n_{\text{crit}}$ , and the light starts to follow the mass, in a pattern similar to that for CO. Although Figure 1 shows only the intermediate case, the normal galaxy and starburst cases give qualitatively identical results. This confirms the intuitive argument given in § 1: *high critical density transitions trace regions of similar density in every galaxy, while low critical density transitions trace regions whose density is close to the median density.*

Now consider how the luminosity in a given line correlates with the star formation rate in galaxies of varying mean densities. For a given  $\bar{n}$ , we can compute the volume density of star formation from equation (2) and the line luminosity density from equation (9). To facilitate comparison with observations, rather than considering the total line luminosity, we use the quantity  $L'$  (Solomon et al. 1997), which is related to the luminosity  $L$  by

$$L' = \frac{c^2}{8\pi k_B \nu^2} L, \quad (10)$$

converted to the units  $\text{K km s}^{-1} \text{ pc}^2$ .

Similarly, we can estimate the far-infrared luminosity from the star formation rate. There is a tight correlation between far-IR emission and star formation, particularly for dense, dusty galaxies like those that make up most of the dynamic range of the Kennicutt (1998a) sample. To the extent that most or all of the light from young stars is reprocessed by dust before escaping the galaxy, the bolometric luminosity integrated over the wavelength range

8–1000  $\mu\text{m}$ , which we define as  $L_{\text{FIR}}$ , simply provides a calorimetric measurement of the total energy output by young stars and is therefore an excellent tracer of recent star formation (Sanders & Mirabel 1996; Rowan-Robinson et al. 1997; Kennicutt 1998a, 1998b; Hirashita et al. 2003; Bell 2003; Iglesias-Páramo et al. 2006). We therefore estimate the FIR luminosity from the star formation rate via

$$L_{\text{FIR}} = \epsilon \dot{M}_* c^2, \quad (11)$$

where  $\epsilon$  is an IMF-dependent constant. For consistency with Kennicutt (1998a, 1998b) we take  $\epsilon = 3.8 \times 10^{-4}$ . To be precise and to facilitate comparison with observations, we adopt the Sanders & Mirabel (1996) definition of  $L_{\text{FIR}}$  as a weighted sum of the luminosity in the 60 and 100  $\mu\text{m}$  *IRAS* bands. This definition of the infrared luminosity generically underestimates the total infrared luminosity [8–1000]  $\mu\text{m}$  by a factor of 1.5–2 (Calzetti et al. 2000; Dale et al. 2001; Bell 2003). However, we use the  $\epsilon$  value appropriate for  $L_{\text{FIR}}$  rather than for the total IR luminosity because some of the observations to which we wish to compare our model (see § 3.3) provide only  $L_{\text{FIR}}$ . Note that this choice for the connection between the star formation rate and the infrared luminosity is not fully consistent with our choice of the gas temperature for the three sets of parameters—normal, intermediate, and starburst—listed in Table 1, an issue we discuss in more detail in § 4.3.

We plot the ratio of star formation rate to line luminosity, and infrared luminosity to line luminosity, as a function of  $\bar{n}$  in Figure 2. First consider the top panel, which shows all three lines computed for the intermediate case. This again confirms our intuitive argument. Since the luminosity per unit volume in the CO line is roughly proportional to the mass density, and the star formation rate/IR luminosity is proportional to mass density to the 1.5 power, the ratios  $\dot{M}_*/L'$  and  $L_{\text{FIR}}/L'$  vary roughly as  $\bar{n}^{0.5}$ . A power-law fit to the data over the range shown in Figure 2 gives an index of 0.57. In contrast, the ratio of star formation density to HCN luminosity density is nearly constant for galaxies with  $\bar{n} < 10^3 \text{ cm}^{-3}$ , and varies quite weakly with  $\bar{n}$  up to densities of  $10^4 \text{ cm}^{-3}$ , values found in the densest starbursts. A power-law fit from  $10 \text{ cm}^{-3}$  to  $10^4 \text{ cm}^{-3}$  gives an index of 0.17; from  $10 \text{ cm}^{-3}$  and  $10^3 \text{ cm}^{-3}$ , the best-fit power-law index is 0.08. As in Figure 1, the slope of the  $\dot{M}_*/L'$  curve for  $\text{HCO}^+$  represents an intermediate case, with a roughly constant ratio of  $\dot{M}_*/L'$  and  $L_{\text{FIR}}/L'$  at low  $\bar{n}$ , rising to a slope comparable to that for CO at high values of  $\bar{n}$ .

Now consider the bottom three panels in Figure 2. Each panel shows the ratio of star formation rate and infrared luminosity to line luminosity for a single line, computed for each of the three galaxy models. The most important point to take from these plots is that the choice of galaxy model has little effect in most cases. The largest differences are for HCN, where at  $\bar{n} = 10 \text{ cm}^{-3}$  the IR to line ratio predicted for the intermediate case differs from the normal galaxy case by a factor of 6.1, and from the starburst case by a factor of 4.1. This variation comes primarily from changes in the Mach number and the optical depth between models. The higher Mach number of the starburst model significantly increases the amount of mass in the high overdensity tail of the probability distribution, while the higher optical depth lowers the effective critical density. Both of these effects increase the amount of mass dense enough to emit in  $\text{HCN}(1 \rightarrow 0)$  and reduce  $\dot{M}_*/L'$ . At higher mean densities these effects become less important and the models converge, so that by  $\bar{n} = 10^4 \text{ cm}^{-3}$  the range in  $\dot{M}_*/L'$  from the normal to the starburst case is only a factor of 3.5.

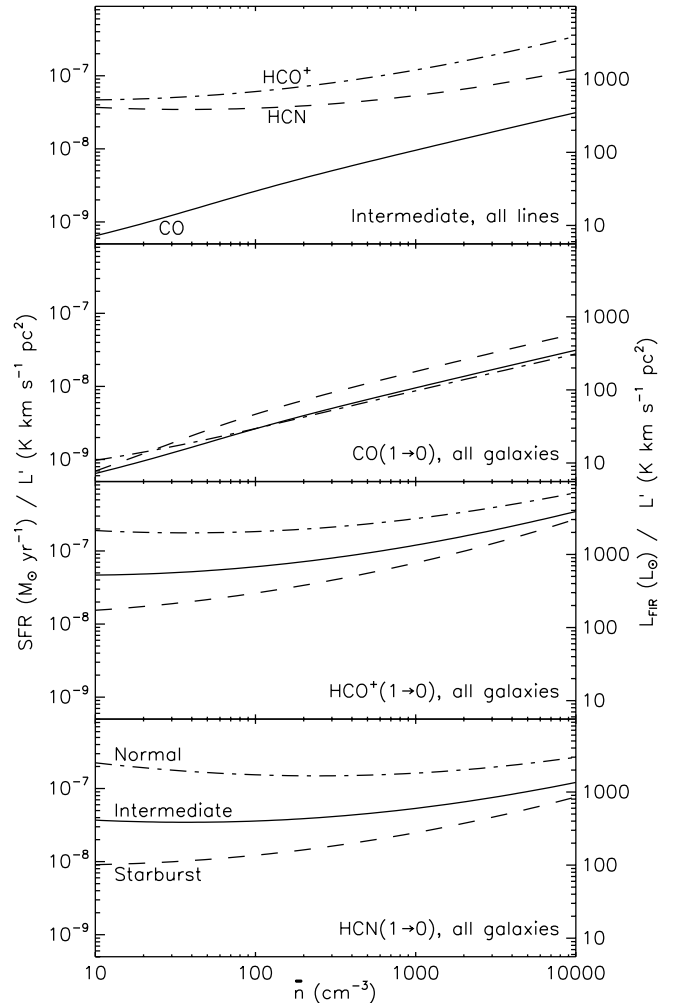


FIG. 2.—Ratio of star formation rate or infrared luminosity to line luminosity, as a function of mean density  $\bar{n}$ . In the top panel we show the lines  $\text{CO}(1 \rightarrow 0)$  (solid line),  $\text{HCO}^+(1 \rightarrow 0)$  (dot-dashed line), and  $\text{HCN}(1 \rightarrow 0)$  (dashed line) for the intermediate case in Table 1. In the next three panels we show the  $\text{CO}(1 \rightarrow 0)$ ,  $\text{HCO}^+(1 \rightarrow 0)$ , and  $\text{HCN}(1 \rightarrow 0)$  lines for the normal galaxy case (dotted-dashed line), intermediate case (solid line), and starburst case (dashed line).

Most importantly, our central conclusion that  $\dot{M}_*/L'_{\text{HCN}}$  is roughly constant across galaxies, while  $\dot{M}_*/L'_{\text{CO}}$  rises as roughly  $[L'_{\text{CO}}]^{0.5}$ , still holds when we consider how conditions vary across galaxies. Galaxies with low mean densities  $\bar{n}$  are generally closest to the normal galaxy case, while those with high mean densities should be closest to the starburst case, and this systematic variation in galaxy properties with  $\bar{n}$  still leaves  $\dot{M}_*/L'$  relatively flat for HCN, and varying with a slope close to 0.5 for CO. From the normal galaxy case at  $\bar{n} = 10 \text{ cm}^{-3}$  to the starburst case at  $\bar{n} = 10^4 \text{ cm}^{-3}$ , the value of  $\dot{M}_*/L'$  varies by more than a factor of 50 for  $\text{CO}(1 \rightarrow 0)$ , but by less than a factor of 3 for the  $\text{HCN}(1 \rightarrow 0)$ .

### 3.3. Comparison with Observations

The calculations illustrated in Figure 2 demonstrate the basic argument that one expects a roughly constant star formation rate per unit line luminosity for high-density tracers (e.g., HCN), and a star formation rate per unit luminosity that rises like luminosity to the  $\sim 0.5$  power for low-density tracers (e.g., CO). However, in large surveys one cannot always determine the mean density in a galaxy, which would be required to construct an observational analog to Figure 2. Instead, we can use our calculated dependence of star formation rate and line luminosity on density to compare to



- Solomon, P. M., Downes, D., Radford, S. J. E., & Barrett, J. W. 1997, *ApJ*, 478, 144
- Solomon, P. M., Rivolo, A. R., Barrett, J., & Yahil, A. 1987, *ApJ*, 319, 730
- Solomon, P. M., & Vanden Bout, P. A. 2005, *ARA&A*, 43, 677
- Tafalla, M., Myers, P. C., Caselli, P., & Walmsley, C. M. 2004a, *A&A*, 416, 191
- . 2004b, *Ap&SS*, 292, 347
- Thompson, T. A., Quataert, E., & Murray, N. 2005, *ApJ*, 630, 167
- Wada, K., & Norman, C. 2007, *ApJ*, 660, 276
- Weiß, A., Downes, D., Neri, R., Walter, F., Henkel, C., Wilner, D. J., Wagg, J., & Wiklind, T. 2007, *A&A*, 467, 955
- Weiß, A., Downes, D., Walter, F., & Henkel, C. 2005, *A&A*, 440, L45
- Weiß, A., Henkel, C., Downes, D., & Walter, F. 2003, *A&A*, 409, L41
- Wild, W., Harris, A. I., Eckart, A., Genzel, R., Graf, U. U., Jackson, J. M., Russell, A. P. G., & Stutzki, J. 1992, *A&A*, 265, 447
- Wong, T., & Blitz, L. 2002, *ApJ*, 569, 157
- Wu, J., Evans, N. J., Gao, Y., Solomon, P. M., Shirley, Y. L., & Vanden Bout, P. A. 2005, *ApJ*, 635, L173
- Yao, L., Seaquist, E. R., Kuno, N., & Dunne, L. 2003, *ApJ*, 588, 771
- Zaritsky, D., Kennicutt, R. C., Jr., & Huchra, J. P. 1994, *ApJ*, 420, 87





